Unusually Slow Photodissociation of CO from (η^6-C_6H_6)Cr(CO)$_3$ (M = Cr or Mo): A Time-Resolved Infrared, Matrix Isolation, and DFT Investigation

Mohammed A. H. Alamiry,[†,‡] Nicola M. Boyle,[‡] Christopher M. Brookes,[§]
Michael W. George,[*,§] Conor Long,[*,‡] Peter Portius,[§,⊥] Mary T. Pryce,[‡] Kate L. Ronayne,[△]
Xue-Zhong Sun,[§] Michael Towrie,[△] and Khuong Q. Vuong[§]

Department of Chemistry, University of Nottingham, Nottingham NG7 2RD, U.K., and School of Chemical Sciences, Dublin City University, Dublin 9, Ireland

Received October 22, 2008

The photochemistry of (η^6-C_6H_6)M(CO)$_3$ (M = Cr or Mo) is described. Photolysis with $\lambda_{exc.} > 300$ nm of (η^6-C_6H_6)Cr(CO)$_3$ in low-temperature matrixes containing CO produced the CO-loss product, while lower energy photolysis ($\lambda_{exc.} > 400$ nm) produced Cr(CO)$_6$. Pulsed photolysis ($\lambda_{exc.} = 400$ nm) of (η^6-C_6H_6)Cr(CO)$_3$ in *n*-heptane solution at room temperature produced an excited-state species (1966 and 1888 cm^{-1}) that decays over 150 ps to (η^6-C_6H_6)Cr(CO)$_2$(*n*-heptane) (70%) and (η^6-C_6H_6)Cr(CO)$_3$ (30%). Pulsed photolysis ($\lambda_{exc.} = 266$ nm) of (η^6-C_6H_6)Cr(CO)$_3$ in *n*-heptane produced bands assigned to (η^6-C_6H_6)Cr(CO)$_2$(*n*-heptane) (1930 and 1870 cm^{-1}) within 1 ps. These bands increase with a rate identical to the rate of decay of the excited-state species and the rate of recovery of (η^6-C_6H_6)Cr(CO)$_3$. Photolysis of (η^6-C_6H_6)Mo(CO)$_3$ at 400 nm produced an excited-state species (1996 and 1898 cm^{-1}) and traces of (η^6-C_6H_6)Mo(CO)$_2$(*n*-heptane) within 1 ps. For the chromium system CO-loss can occur following excitation at both 400 and 266 nm via an avoided crossing of a MACT (metal-to-arene charge transfer) and MCCT/LF (metal-to-carbonyl charge transfer/ligand field) states. This leads to an unusually slow CO-loss following excitation with 400 nm light. Rapid CO-loss is observed following 266 nm excitation because of direct population of the MCCT/LF state. The quantum yield for CO-loss in the chromium system decreases with increasing excitation energy because of the competing population of a high-energy unreactive MACT state. For the molydenum system CO-loss is a minor process for 400 nm excitation, and an unreactive MACT state is evident from the TRIR spectra. A higher quantum yield for CO-loss is observed following 266 nm excitation through both direct population of the MCCT/LF state and production of a vibrationally excited reactive MACT state. This results in the quantum yield for CO-loss increasing with increasing excitation energy.

Organometallic complexes have many uses in catalytic and synthetic systems, and (η^6-C_6H_6)Cr(CO)$_3$ complexes have found many applications in organic syntheses.[1,2] The coordination of an arene to a Cr(CO)$_3$ fragment can activate the arene toward nucleophilic attack,[1] enhance the kinetic acidity of the ring hydrogens,[3] increase the stability of anionic intermediates,[4] and also impart some regiocontrol in substitution reactions.[5] The ability of the arene ligand to undergo ring-slip or haptotropic shift processes has also been implicated in some nucleophilic substitution reactions.[6]

Although there have been extensive investigations, the precise mechanism of the arene exchange reaction in (η^6-C_6H_6)Cr(CO)$_3$ complexes is still under debate. Proposals ranging from self-catalysis,[7−9] to CO-loss,[10,11] to a stepwise ring displacement process have been presented.[6,12] The latter hypothesis involved an η^6 to η^4 haptrotropic shift preceding coordination of the entering arene ligand. A recent theoretical study that examined

---

[*] To whom correspondence should be addressed. E-mail: Mike.George@nottingham.ac.uk; Conor.Long@dcu.ie.

[†] Present address: Molecular Photonics Laboratory, School of Natural Sciences, Bedson Building, University of Newcastle, Newcastle upon Tyne NE1 7RU, UK.

[‡] Dublin City University.

[§] University of Nottingham.

[⊥] Department of Chemistry, University of Sheffield, Sheffield S3 7HF, England.

[△] Central Laser Facility, Photon Science Department, Science & Technology Facilities Council, Rutherford Appleton Laboratory, Harwell Science and Innovation Campus, Didcot, Oxfordshire, OX11 0QX, UK.

(1) Djukic, J. P.; Rosemunch, F.; Rose, E.; Simon, F.; Dromzee, Y. *Organometallics* **1995**, *14*, 2027–2038.

(2) McQuillin, F. J.; Parker, D. G.; Stephenson, G. R. *Transition Metal Organometallics for Organic Synthesis*; Cambridge University Press: Cambridge, UK, 1991.

(3) Card, R. J.; Trahanovsky, W. S. *J. Org. Chem.* **1980**, *45*, 2555–2559.

(4) Semmelhack, M. F.; Hall, H. T.; Yoshifuji, M.; Clark, G. *J. Am. Chem. Soc.* **1975**, *97*, 1247–1248.

(5) Semmelhack, M. F.; Garcia, J. L.; Cortes, D.; Farina, R.; Hong, R.; Carpenter, B. K. *Organometallics* **1983**, *2*, 467–469.

(6) Zingales, F.; Chiesa, A.; Basolo, F. *J. Am. Chem. Soc.* **1966**, *88*, 2707–2710.

(7) Strohmeier, W.; Mittnacht, H. Z. *J. Phys. Chem. (Muenchen)* **1961**, *29*, 339–346.

(8) Strohmeier, W.; Staricco, E. H. *J. Phys. Chem. (Muenchen)* **1963**, *38*, 315–325.

(9) Strohmeier, W.; Muller, R. J. *J. Phys. Chem. (Muenchen)* **1964**, *40*, 85–95.

(10) Wrighton, M. S.; Haverty, J. L. *Z. Naturforsch.* **1975**, *30* (b), 254–258.

(11) Strohmeier, W.; von Hobe, D. Z. *Z. Naturforsch.* **1963**, *18* (b), 770–771.

(12) Traylor, T. G.; Stewart, K. J. *J. Am. Chem. Soc.* **1986**, *108*, 6977–6985.

10.1021/om800925s CCC: $40.75

various reduced hapticity species indicated that (η^4-C_6H_6)-$Cr(CO)_3$ is not at a minimum on either the ground-state singlet or triplet potential energy hypersurfaces.[13] However a number of other reduced hapticity species were found, including (η^2-C_6H_6)$Cr(CO)_3$ and (η^1-C_6H_6)$Cr(CO)_3$.

The combination of photochemistry and time-resolved spectroscopy is a powerful tool for probing ligand substitutions and reaction mechanisms. The photochemistry of (η^6-C_6H_6)$Cr(CO)_3$ has also been extensively investigated; the dominant photochemical process is CO-loss.[14−20] The high quantum efficiency ($\Phi_{CO} = 0.72$) of this process has been reported to be independent of excitation wavelength at room temperature,[10] although close inspection of the published data does reveal a small wavelength-dependent effect, which is particularly relevant to this work (see below). In contrast, the quantum efficiency of CO-loss in the molybdenum analogue shows a marked wavelength dependence (Φ_{CO} increases with increasing excitation energy), and the tungsten complex appears to be photochemically inert in hydrocarbon solvents.[21] Photoinduced arene exchange was also observed for (η^6-C_6H_6)$Cr(CO)_3$ under appropriate conditions (see above).[22] A number of intriguing observations were made for this process. For instance addition of CO to the photolysis solution suppresses arene exchange. Also the quantum efficiency of the arene exchange process is strongly solvent dependent.[23] Intermediates in the photoinduced arene exchange process remain elusive for (η^6-arene)$Cr(CO)_3$ systems with one exception. Low-energy photolysis of (η^6-C_5H_5N)$Cr(CO)_3$ produced the haptotropic shift product (η^1-*N*-C_5H_5N)$Cr(CO)_3$.[24,25] Many questions remain unanswered, and the application of fast time-resolved spectroscopic techniques offers the opportunity to address some of these issues.

The published studies of particular relevance to this work are (i) the now generally accepted mechanism for CO-loss from homoleptic group 6 carbonyls, which involves vibronic coupling in the initially produced excited state, leading to an unbound state with respect to the M−CO interaction and fast (~100 fs) expulsion of one CO ligand,[26,27] (ii) the photoinduced CO substitution in $M(CO)_4$(α-diimine) complexes (M = Cr, Mo, or W), which involves independent reactions from at least two different metal to ligand charge transfer (MLCT) excited states,[28] and (iii) the recent observation of slow CO-loss from an avoided crossing of a thermally relaxed ^{3}MLCT/XLCT (metal-to-ligand/halide-to-ligand charge transfer) excited state following irradiation of [$RuCl_2(CO)_2$(^{i}Pr-dab)] (^{i}Pr-dab = *N,N′*-diisopropyl-1,4-diazabutadiene).[29] In this paper we report an investigation into the photochemistry of (η^6-C_6H_6)$M(CO)_3$ systems (M = Cr or Mo) using picosecond time-resolved infrared spectroscopy and matrix isolation techniques in order to gain a greater insight into the underlying photophysical processes preceding either CO-loss or arene exchange. We monitor the decay of an excited-state precursor to the CO-loss process and show that CO-loss is slow because of an avoided crossing.

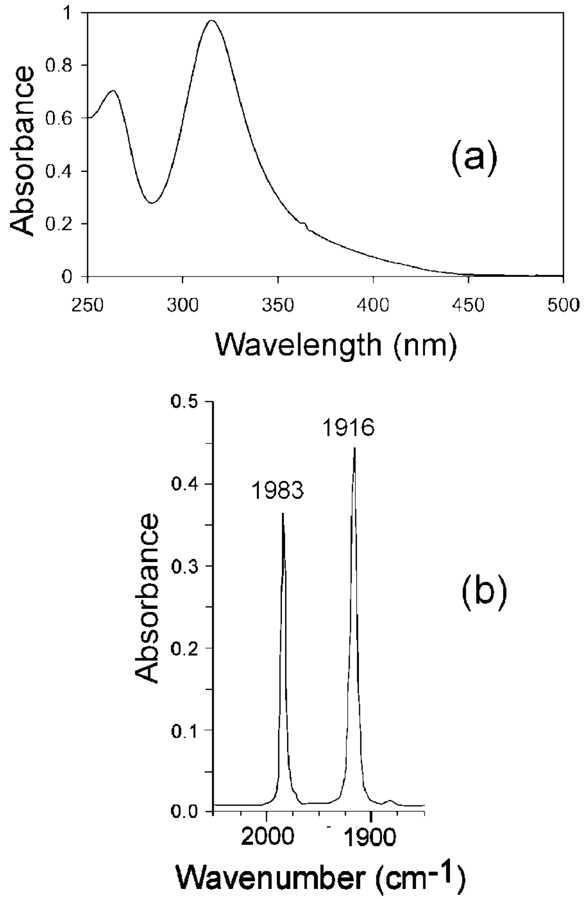

Figure 1. (a) Ground-state UV/vis spectrum of (η^6-C_6H_6)$Cr(CO)_3$ in cyclohexane at room temperature. (b) Ground-state IR spectrum (ν_{CO} region) of (η^6-C_6H_6)$Cr(CO)_3$ in *n*-heptane at room temperature.

Results

The UV/vis and IR spectra of (η^6-C_6H_6)$Cr(CO)_3$ are presented in Figure 1, and Table 1 contains spectroscopic information for the complexes in this study. The time-resolved and matrix isolation spectra are presented in the form of difference absorbance in which the positive (upward) peaks represent the appearance of new species, while negative (downward bleaches) peaks represent photoinduced depletion.

Matrix Photochemistry of (η^6-C_6H_6)$Cr(CO)_3$. (η^6-C_6H_6)-$Cr(CO)_3$ was deposited in a low-temperature (12 K) frozen gas

---

(13) Cohen, R.; Weitz, E.; Martin, J. M. L.; Ratner, M. A. *Organometallics* **2004**, *23*, 2315–2325.

(14) Strohmeier, W. *Angew. Chem., Int. Ed.* **1964**, *3*, 730.

(15) Black, J. D.; Boylan, M. J.; Braterman, P. S. *J. Chem. Soc., Dalton Trans.* **1981**, *673*, 677.

(16) Wang, W. P.; Parr, R. G.; Murphy, D. R.; Henderson, G. A. *Chem. Phys. Lett.* **1976**, *43*, 409–412.

(17) Wang, W. H.; Jin, P.; Liu, Y. W.; She, Y. B.; Fu, K. J. *Chin. Phys. Lett.* **1991**, *8*, 491–494.

(18) Wang, W. H.; Jin, P.; Liu, Y. W.; She, Y. B.; Fu, K. J. *J. Phys. Chem.* **1992**, *96*, 1278–1283.

(19) Hill, R. H.; Wrighton, M. S. *Organometallics* **1987**, *6*, 632–638.

(20) To, T. T.; Heilweil, E. J.; Burkey, T. J. *J. Phys. Chem. A* **2006**, *110*, 10669–10673.

(21) Breheny, C. J.; Kelly, J. M.; Long, C.; O'Keefe, S.; Pryce, M. T.; Russell, G.; Walsh, M. M. *Organometallics* **1998**, *17*, 3690–3695.

(22) Gilbert, A.; Kelly, J. M.; Budzwatt, M.; Koerner von Gustorf, E. *Z. Naturforsch.* **1976**, *31* (b), 1091.

(23) Brennan, P.; George, M. W.; Jina, O. S.; Long, C.; McKenna, J.; Pryce, M. T.; Sun, X.-Z.; Khuong Q. Vuong, K. Q. *Organometallics* **2008**, *27*, 3671–3680.

(24) Breheny, C. J.; Draper, S. M.; Grevels, F. W.; Klotzbucher, W. E.; Long, C.; Pryce, M. T.; Russell, G. *Organometallics* **1996**, *15*, 3679–3687.

(25) Draper, S. M.; Byrne, J. J.; Breheny, C. J.; Long, C.; Low, J. N. *Acta Crystallogr., Sect. C: Cryst. Struct. Commun.* **1994**, *50*, 1669–1671.

(26) Pollak, C.; Rosa, A.; Baerends, E. J. *J. Am. Chem. Soc.* **1997**, *119*, 7324–7329.

(27) Rosa, A.; Baerends, E. J.; van Gisbergen, S. J. A.; van Lenthe, E.; Groeneveld, J. A.; Snijders, J. G. *J. Am. Chem. Soc.* **1999**, *121*, 10356–10365.

(28) Vlcek, A. *Coord. Chem. Rev.* **2002**, *230*, 225–242.

(29) Gabrielsson, A.; Towrie, M.; Zalis, S.; Vlcek, A. *Inorg. Chem.* **2008**, *47*, 4236–4242.

Table 1. Observed ν_{CO} Peak Positions for Complexes in This Study

complex	state	wavenumber (cm^{-1})		medium
(η^6-C_6H_6)Cr(CO)$_3$	GS[a]	1983	1916	*n*-heptane
(η^6-C_6H_6)Mo(CO)$_3$	GS[a]	1987	1916	*n*-heptane
Cr(CO)$_6$	GS[a]	1984		CH_4 matrix
(η^6-C_6H_6)Cr(CO)$_3$	MACT$_1$[b]	1966	1888	*n*-heptane
(η^6-C_6H_6)Mo(CO)$_3$	MACT$_1$[b]	1966	[d]	*n*-heptane
(η^6-C_6H_6)Mo(CO)$_3$	MACT$_2$[c]	1996	1894	*n*-heptane
(η^6-C_6H_6)Cr(CO)$_2$(*n*-heptane)	GS[a]	1930	1870	*n*-heptane
(η^6-C_6H_6)Mo(CO)$_2$(*n*-heptane)	GS[a]	1933	1876	*n*-heptane

[a] GS = ground state. [b] MACT$_1$ = metal-to-ligand charge transfer type 1. [c] MACT$_2$ = metal-to-ligand charge transfer type 2 (see text for details). [d] Band obscured by the MACT$_2$ band of (η^6-C_6H_6)Mo(CO)$_3$.

Scheme 1. Proposed Photochemical Behavior of (η^6-C_6H_6)-M(CO)$_3$ (M = Cr or Mo) in *n*-Heptane Solution at Room Temperature[a]

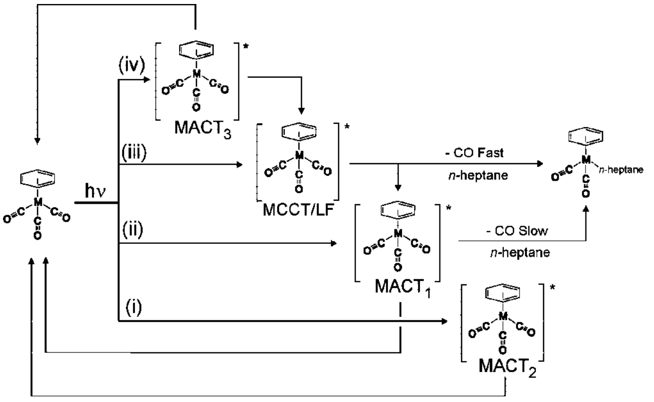

[a] (i) $\lambda_{exc.}$ = 400 nm, M = Mo; (ii) $\lambda_{exc.}$ = 400 nm, M = Cr; $\lambda_{exc.}$ = 266 nm, M = Mo (vibrationally excited); (iii) $\lambda_{exc.}$ = 266 nm, M = Cr or Mo; (iv) $\lambda_{exc.}$ = 266 nm, M = Cr (partial).

matrix consisting of a mixture of 5% CO in CH_4. The IR spectrum of the resulting matrix showed ν_{CO} stretching peaks at 1978 and 1906 cm^{-1}, consistent with the parent tricarbonyl species. The CO was added to the matrix in order to trap any reduced hapticity intermediates that may be produced during photolysis. Irradiation of this matrix with $\lambda_{exc.}$ > 400 nm depleted the peaks of the parent (η^6-C_6H_6)Cr(CO)$_3$ complex and produced new bands at 1982 and 1911 cm^{-1} (Figure 2a). These bands are close to those of the parent complex and are assigned to Cr(CO)$_6$ and possibly a rotamer of (η^6-C_6H_6)Cr(CO)$_3$.[30] Evidence for the formation of Cr(CO)$_6$ comes from an examination of the relative intensities of the parent peaks (Figure 1b). The higher energy symmetric mode in (η^6-C_6H_6)Cr(CO)$_3$ is less intense than the degenerate asymmetric stretch. However the higher energy peak in Figure 2a ($\lambda_{exc.}$ > 400 nm) is significantly more intense than the lower energy peak, indicating the production of Cr(CO)$_6$ (ν_{CO} = 1984 cm^{-1} Scheme 1). In addition to the features described above, weak peaks (1922 and 1867 cm^{-1}) characteristic of the CO-loss species (η^6-C_6H_6)Cr(CO)$_2$ were formed.[31] Increasing the energy of the irradiation ($\lambda_{exc.}$ > 300 nm) resulted in a greater depletion of the parent absorptions for a given irradiation time and an increase in the intensity of the peaks assigned to the CO-loss species (η^6-C_6H_6)Cr(CO)$_2$ and also Cr(CO)$_6$.

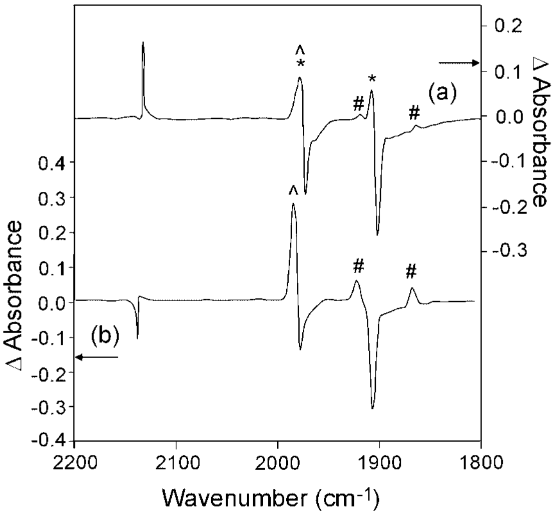

Figure 2. (a) Changes in IR absorption observed following irradiation of a 5% CO in CH_4 matrix containing (η^6-C_6H_6)Cr(CO)$_3$ at 12 K with $\lambda_{exc.}$ > 400 nm for 330 min showing the possible formation of a rotamer of the parent (*), Cr(CO)$_6$ (∧), and weak peaks of the CO-loss species (η^6-C_6H_6)Cr(CO)$_2$ (#). (b) Changes in IR absorption observed following subsequent photolysis ($\lambda_{exc.}$ > 300 nm for 125 min) of the same matrix previously irradiated as in (a) showing the formation of (η^6-C_6H_6)Cr(CO)$_2$ (#) and Cr(CO)$_6$ (∧). Changes in free concentration by reaction to form Cr(CO)$_6$ result in the spectral features at approximately 2143 cm^{-1}.

Picosecond Time-Resolved Infrared (TRIR) Studies. TRIR studies were undertaken on (η^6-C_6H_6)M(CO)$_3$ (M = Cr or Mo) in CO-saturated *n*-heptane solution at room temperature (298 K).

TRIR Studies on (η^6-C_6H_6)Cr(CO)$_3$ ($\lambda_{exc.}$ = 400 nm). Photolysis ($\lambda_{exc.}$ = 400 nm) of (η^6-C_6H_6)Cr(CO)$_3$ depleted the ν_{CO} peaks of (η^6-C_6H_6)Cr(CO)$_3$ within the instrumental time resolution used in these experiments (1 ps), Figure 3a. Two new peaks were formed within 1 ps at 1966 and 1888 cm^{-1}. These bands are to the low-energy side of the parent bands, and this might indicate a change to the coordination mode of the benzene ligand in this species. These two peaks decay over the subsequent 150 ps with concomitant recovery of (η^6-C_6H_6)Cr(CO)$_3$ and production of (η^6-C_6H_6)Cr(CO)$_2$(*n*-heptane) (1930 and 1870 cm^{-1}), which can be assigned by comparison to the previously reported nanosecond TRIR experiments.[32] Approximately 30% of the parent is re-formed following this decay based on examination of the low-energy ν_{CO} band of (η^6-C_6H_6)Cr(CO)$_3$. The 30% recovery of the parent bands is consistent with the published quantum yield for CO-loss from (η^6-arene)Cr(CO)$_3$ of 0.72, which was obtained by averaging the values for arene = C_6H_6 or 1,3,5-$(CH_3)_3C_6H_3$ in isooctane or benzene solvents.[10,22] Thus, it is clear that the initially produced species, absorbing at 1966 and 1888 cm^{-1}, is an intermediate in both the recovery of the parent (η^6-C_6H_6)Cr(CO)$_3$ complex and also the formation of (η^6-C_6H_6)Cr(CO)$_2$(*n*-heptane) (Figure 3b). A comparison of the IR spectrum of the solution before and after photolysis revealed no significant changes in the ν_{CO} region.

TRIR Studies on (η^6-C_6H_6)Cr(CO)$_3$ ($\lambda_{exc.}$ = 266 nm). Photolysis of (η^6-C_6H_6)Cr(CO)$_3$ at higher energy ($\lambda_{exc.}$ = 266 nm) resulted in depletion of the ν_{CO} peaks of the parent complex.

---

(30) Bitterwolf, T. E.; Bays, J. T.; Scallorn, B.; Weiss, C. A.; George, M. W.; Virrels, I. G.; Linehan, J. C.; Yonker, C. R. *Eur. J. Inorg. Chem.* **2001**, *261*, 9–2624.

(31) Rest, A. J.; Sodeau, J. R.; Taylor, D. J. *J. Chem. Soc., Dalton Trans.* **1978**, *651*, 656.

(32) Creaven, B. S.; George, M. W.; Ginzburg, A. G.; Hughes, C.; Kelly, J. M.; Long, C.; McGrath, I. M.; Pryce, M. T. *Organometallics* **1993**, *12*, 3127–3131.

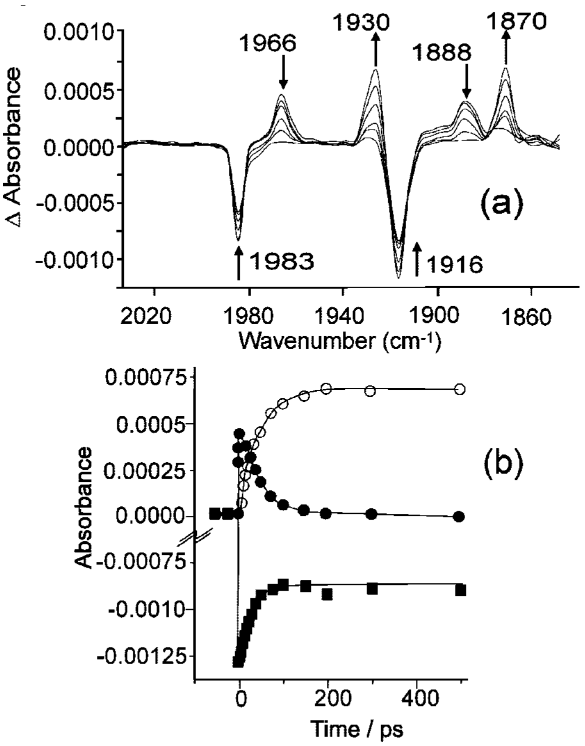

Figure 3. (a) TRIR spectra obtained following pulsed photolysis of $(\eta^6\text{-}C_6H_6)Cr(CO)_3$ in *n*-heptane ($\lambda_{exc.}$ = 400 nm) at room temperature (spectra obtained at 7, 15, 20, 40, 75, and 200 ps) showing depletion of the two peaks of $(\eta^6\text{-}C_6H_6)Cr(CO)_3$ (1983 and 1916 cm^{-1}) and the immediate formation of two peaks at 1966 and 1888 cm^{-1}. The peaks at 1930 and 1870 cm^{-1} increase in intensity over 150 ps; the arrows indicate the temporal behavior of the bands. (b) Plot of the time dependence of the parent peak at 1916 cm^{-1} (■), the peak at 1966 cm^{-1} (●), and the 1930 cm^{-1} peak (○).

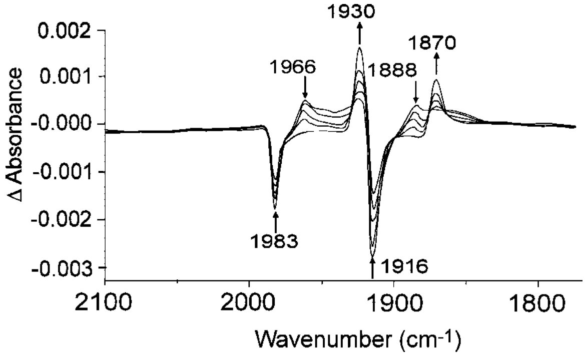

Figure 4. TRIR spectra obtained following photolysis of $(\eta^6\text{-}C_6H_6)Cr(CO)_3$ in CO-saturated *n*-heptane ($\lambda_{exc.}$ = 266 nm) (spectra obtained at 3, 13, 30, 44, and 160 ps after excitation). The arrows describe the temporal behavior of the various bands. Broad peaks of the excited state at 1966 and 1888 cm^{-1} indicate that this species is vibrationally hot when formed. The peaks narrow as they reduce in intensity. Peaks at 1930 and 1870 cm^{-1} show the formation of $(\eta^6\text{-}C_6H_6)Cr(CO)_2$(*n*-heptane) within the response time of the instrument and its subsequent formation over 150 ps.

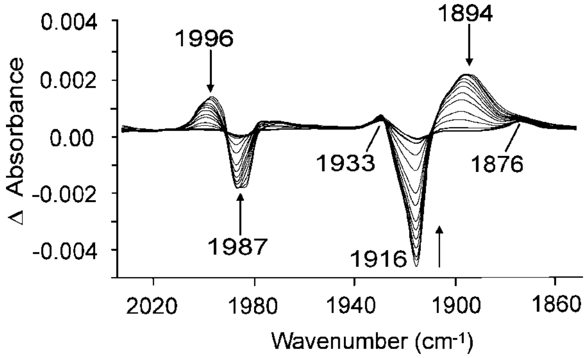

Figure 5. TRIR difference spectra obtained following photolysis of $(\eta^6\text{-}C_6H_6)Mo(CO)_3$ in *n*-heptane (S) at room temperature ($\lambda_{exc.}$= 400 nm) showing formation of two broad peaks of the ^{1}MACT excited state at 1996 and 1894 cm^{-1}, which decay over 150 ps accompanied by almost complete (approximately 93%) recovery of the parent depletion (1987 and 1916 cm^{-1}). Additional small product peaks for $(\eta^6\text{-}C_6H_6)Mo(CO)_2$(*n*-heptane) at 1933 and 1876 cm^{-1} formed within the excitation pulse, and these peaks do not increase over the subsequent 150 ps. The arrows indicate the temporal behavior of the bands.

The bands at 1966 and 1888 cm^{-1} were also observed in the TRIR spectrum obtained 1 ps following excitation. These two features were significantly broader than those produced following 400 nm excitation (cf. Figure 3a and Figure 4). Another important difference between TRIR experiments using different excitation wavelengths is that the CO-loss species, $(\eta^6\text{-}C_6H_6)Cr(CO)_2$(*n*-heptane) (1930 and 1870 cm^{-1}), was formed within 1 ps following 266 nm excitation. These bands increased in intensity over the subsequent 150 ps (Figure 4). A particularly noteworthy observation is that the parent peaks in this experiment recovered by ca. 50%, which is significantly greater than the recovery observed following excitation at 400 nm and implies that the quantum yield for the CO-loss process is smaller at 266 nm than at 400 nm. The observation of a reduction in quantum yield following higher energy excitation was confirmed by our steady-state quantum yield determinations (see below).

TRIR Studies of $(\eta^6\text{-}C_6H_6)Mo(CO)_3$ ($\lambda_{exc.}$ = 400 nm). Photolysis ($\lambda_{exc.}$ = 400 nm) of $(\eta^6\text{-}C_6H_6)Mo(CO)_3$ depleted the parent peaks at 1987 and 1916 cm^{-1}. Two peaks at 1996 and 1894 cm^{-1} were formed within 1 ps (Figure 5). These peaks are significantly broader than those of the parent; they narrow and shift to slightly higher energy as they decay over 150 ps, indicating the formation of this species in a vibrationally excited state, which then relaxes. Concomitant with the decay of these peaks, the parent bleach recovers by approximately 93% and the residual bleach persists for at least 600 ps. It is important to note that two weak features are also formed within the laser pulse at 1933 and 1876 cm^{-1} corresponding to the CO-loss species $(\eta^6\text{-}C_6H_6)Mo(CO)_2$(*n*-heptane). In contrast to the chromium system these peaks do not increase in intensity with time. The formation of $(\eta^6\text{-}C_6H_6)Mo(CO)_2$(*n*-heptane) accounts for the persistent parent bleach and provides an estimate of 0.07 for the CO-loss quantum yield for 400 nm excitation.

TRIR Studies of $(\eta^6\text{-}C_6H_6)Mo(CO)_3$ ($\lambda_{exc.}$ = 266 nm). Irradiation of $(\eta^6\text{-}C_6H_6)Mo(CO)_3$ at 266 nm depleted the parent peaks and produced two very broad peaks at 1971 and 1899 cm^{-1} along with weak features of $(\eta^6\text{-}C_6H_6)Mo(CO)_2$(*n*-heptane) (1933 and 1876 cm^{-1}) within the instrument response time of 1 ps (Figure 6). The broad peaks at 1971 and 1899 cm^{-1} decay over 150 ps with concomitant recovery of the parent bleach (approximately 60%) and a growth of the bands of $(\eta^6\text{-}C_6H_6)Mo(CO)_2$(*n*-heptane). In addition a persistent feature appears at 1966 cm^{-1}. The ultimate yield of $(\eta^6\text{-}C_6H_6)Mo(CO)_2$(*n*-heptane) is greater in these experiments compared to those where 400 nm excitation was used.

Time-Dependent Density Functional Calculations. Density functional theory (DFT) calculations were undertaken on $(\eta^6\text{-}C_6H_6)Cr(CO)_3$ to provide information on the electronic and molecular structures for use in subsequent time-dependent

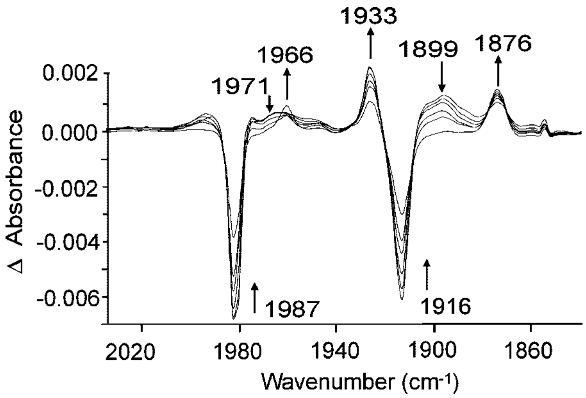

Figure 6. TRIR spectra obtained following photolysis of (η^6-C_6H_6)Mo(CO)$_3$ at 266 nm. Spectra were recorded at 7,16,19, 30, 44, and 160 ps after the excitation pulse. Arrows indicate the temporal behavior of the bands. Very broad features of an excited state are centered at 1971 and 1899 cm^{-1}. Peaks corresponding to (η^6-C_6H_6)Mo(CO)$_2$(*n*-heptane) (1933 and 1876 cm^{-1}) form within the laser pulse and increase in intensity over the subsequent 150 ps. A peak at 1966 cm^{-1} also forms on this time scale. Examination of the high-energy band of (η^6-C_6H_6)Mo(CO)$_3$ at 1987 cm^{-1} indicates a 60% recovery within 600 ps.

Table 2. Vertical Excitation Energy (eV) and Equivalent Photon Wavelength (nm), Oscillator Strengths, and Prevailing Character for the Accessible Excited States of (η^6-C_6H_6)Cr(CO)$_3$ as Calculated by Time-Dependent Density Functional Theory (only transitions with oscillator strengths >1 × 10^{-4} are included)

energy eV (nm)	oscillator strength × 10^3	prevailing character[a]
3.2826 (377.70)	1.4	MACT$_1$[b]
3.2827 (377.69)	1.4	MACT$_1$
3.4569 (358.66)	1.6	MACT$_2$
3.4570 (358.64)	1.6	MACT$_2$
3.5966 (344.73)	1.3	MACT$_2$
3.5967 (344.71)	1.3	MACT$_2$
3.9892 (310.80)	1.5	MCCT[c]/LF[d]
3.9892 (310.79)	1.5	MCCT/LF
4.1654 (297.65)	189.3	MACT$_3$[b]

[a] Numeric subscripts are used to distinguish between different transitions within a given manifold. [b] Metal to arene charge transfer. [c] Metal to carbonyl charge transfer. [d] Ligand field transitions.

density functional theory calculations (TDDFT). A starting geometry was obtained from molecular mechanics calculations on (η^6-C_6H_6)Cr(CO)$_3$. This geometry was then optimized using tight convergence targets at the B3LYP/LANL2DZ+P model chemistry. The final structural parameters were consistent with published values (see Supporting Information). The 20 lowest excited states were characterized by TDDFT. Table 2 contains information on the optically accessible excited states along with their prevailing character defined in terms of the general electron drift, either toward the metal-arene (MACT) fragment or toward the metal-CO fragment (MCCT) (see Supporting Information for more details). It should be noted that all of these states derive from multiple transitions, and the MCCT transitions also contain significant ligand field (LF) character. The manifold of MCCT/LF transitions lies between two MACT manifolds.

Quantum Yield Measurement of Photoinduced CO-Loss from (η^6-C_6H_6)Cr(CO)$_3$. The quantum yield of the photoinduced expulsion of CO from (η^6-C_6H_6)Cr(CO)$_3$ was measured in cyclohexane solution at 298 K. These experiments were undertaken to explain the apparent difference in the recovery of (η^6-C_6H_6)Cr(CO)$_3$ following excitation at 400 and 266 nm in the TRIR experiments. Ferrioxalate actinometry was used to measure the incident light intensity. Measurements were made using two excitation wavelengths of 366 and 265 nm, and cyclooctene was used as a trapping ligand for the photoproduced (η^6-C_6H_6)Cr(CO)$_2$ species (see Experimental Section and Supporting Information for more details). A 200 W Hg−Xe arc lamp was used for these studies, and the required Hg spectral line was selected using interference filters. These excitation wavelengths were selected because they are those close to the excitation wavelengths used in the TRIR experiments with reasonable intensities. The quantum yields measured showed wavelength dependence with values of 0.71 for 366 nm and 0.56 for 265 nm excitation, respectively.

Discussion

It is clear from Figure 1 that irradiation of (η^6-C_6H_6)Cr(CO)$_3$ with $\lambda_{\text{exc.}} = 400$ nm represents photolysis at the low-energy region of the absorption profile, which will populate its low-energy excited states. The results of the TDDFT calculations suggest that the lowest energy transition (377 nm) has a metal to arene charge transfer character (Table 2), the charge drifting from the Cr(CO)$_3$ fragment to the benzene ligand (labeled MACT). However there are other transitions between 344 and 359 nm, and these also have MACT character. To distinguish between these two sets of MACT transitions, we label the transition at 377 nm MACT$_1$ and the higher energy transitions MACT$_2$ in Table 2. Transitions that contain significant ligand field along with metal to CO charge transfer character are predicted at approximately 313 nm (labeled MCCT/LF in Table 2). Finally a high-energy MACT transition was calculated at 297 nm, and this is labeled MACT$_3$.

Under $\lambda_{\text{exc.}} > 400$ nm irradiation of (η^6-C_6H_6)Cr(CO)$_3$, the low-temperature matrix experiments provide evidence for the formation of a rotamer and Cr(CO)$_6$ by reaction with CO present in the matrix. The formation of Cr(CO)$_6$ suggests that CO is trapping either an arene-loss or a reduced hapticity intermediate. Decreasing the irradiation wavelength to $\lambda_{\text{exc.}} > 300$ nm increased the yield of the CO-loss species. This result appears not to be consistent with the published room-temperature quantum yield measurements, which indicate that the efficiency of photochemical loss of CO from (η^6-C_6H_6)Cr(CO)$_3$ is independent of excitation wavelength.[11] The quantum yields of CO-loss from (η^6-C_6H_6)Cr(CO)$_3$ were measured for excitation wavelengths of 366 and 265 nm, and values of 0.71 and 0.56, respectively, were obtained, which indicate that there is in fact a significant wavelength dependence for CO-loss. We interpret that these results mean that there is a difference between the behavior of (η^6-C_6H_6)Cr(CO)$_3$ in a low-temperature matrix and its behavior in room-temperature solution.

Time-resolved infrared spectroscopy following irradiation at 400 nm shows that there is a precursor to CO-loss characterized by two ν_{CO} bands at 1966 and 1888 cm^{-1}. This species cannot be a dicarbonyl since it decays to re-form the parent within 150 ps, and it could not react with CO on this time scale even at the diffusion-controlled limit. This species is therefore assigned to be an excited state. The rate of formation of the CO-loss species, (η^6-C_6H_6)Cr(CO)$_2$ (50−100 ps), is very slow and indicates that there is a thermal barrier for this process. It should be noted that the kinetic data for the decay of the excited state relates to the competing decay routes for the excited state and not the reaction of (η^6-benzene)Cr(CO)$_2$ with the solvent. It is likely that the reaction of (η^6-benzene)Cr(CO)$_2$ with *n*-heptane will be very fast (<1 ps).[33] To the best of our knowledge, there is only one other example of such a slow CO-loss from an

---

[33] Simon, J. D.; Xie, X. L. *J. Phys. Chem.* **1987**, *91*, 5538–5540.

excited state, which was published during the preparation of this article.[29] Vlcek and co-workers demonstrated that slow CO-loss in [RuCl$_2$(CO)$_2$(^{i}Pr-dab)] arose because of an avoided crossing of a thermally relaxed ^{3}MLCT/XLCT excited state. Our results on (η^6-C$_6$H$_6$)Cr(CO)$_3$ for 400 nm excitation are interpreted in terms of formation of an excited state that either decays to the parent or via an avoided crossing with a higher energy excited-state ultimately leads to CO-loss (reaction (i) in Scheme 1). The TDDFT calculations allow tentative assignments of these lower and higher excited states to MACT$_1$ and MCCT/LF, respectively. The ν_{CO} bands of the excited state are shifted to lower wavenumbers than the parent bands. A transfer of electron density from the metal to the arene ligand would be expected to cause a shift of the ν_{CO} bands to higher wavenumbers. However either a significant change to the coordination mode of the arene ligand or a reduction of the arene ligand's π-acceptor capacity could explain the observed shifts.

There are two important differences in the behavior of (η^6-C$_6$H$_6$)Cr(CO)$_3$ following 266 nm compared to 400 nm excitation. First the CO-loss species (η^6-C$_6$H$_6$)Cr(CO)$_2$ is formed via two processes: the CO loss species is observed immediately (1 ps) and then grows as the excited-state bands at 1966 and 1888 cm^{-1} decay. Second the recovery of the parent is higher and the quantum yield of CO-loss is lower following 266 nm compared to 400 nm irradiation. These results support our model of a manifold of MACT and MCCT/LF excited states governing the photochemistry of (η^6-C$_6$H$_6$)Cr(CO)$_3$ as 266 nm directly populates the MCCT/LF state (reaction (iii) in Scheme 1), leading to rapid CO-loss and formation of the MACT$_1$ state. The MACT$_1$ state then decays via an avoided crossing to the MCCT/LF state, resulting in two pathways for the formation of the CO-loss species. The TDDFT calculations also predict a higher energy MACT$_3$ excited state separate from the low-energy MACT manifold. The quantum yield results and the parent re-formation data obtained in the TRIR experiments show the yield of CO-loss decreases with increasing photolysis energy. We interpret this to indicate that three excited states are required to account for the observed photochemical behavior of (η^6-C$_6$H$_6$)Cr(CO)$_3$. The partial population of a high-energy nonreactive MACT$_3$ excited state (reaction (iv) in Scheme 1) at the expense of the reactive MCCT/LF state (reaction (iii) in Scheme 1) would reduce the quantum yield of the CO-loss process.

We now consider the TRIR data obtained for (η^6-C$_6$H$_6$)Mo(CO)$_3$ using $\lambda_{exc.}$= 400 nm. In these experiments bands at 1996 and 1894 cm^{-1} are formed within 1 ps and are assigned to an excited state (reaction (i) in Scheme 1). Additional very small features of (η^6-C$_6$H$_6$)Mo(CO)$_2$(*n*-heptane) are also present in the 1 ps TRIR spectrum. The excited state decays over 150 ps, regenerating (η^6-C$_6$H$_6$)Mo(CO)$_3$ with no further production of (η^6-C$_6$H$_6$)Mo(CO)$_2$(*n*-heptane), clearly demonstrating that the CO-loss product is not formed from the excited state characterized by ν_{CO} bands at 1996 and 1894 cm^{-1} and must be produced from a different excited state.

The measured quantum yield (Φ_{CO}) for loss of CO from (η^6-1,3,5-(CH$_3$)$_3$C$_6$H$_3$)Mo(CO)$_3$ is strongly wavelength dependent and increases with reducing excitation wavelength (0.58, 0.12, and 0.05 for $\lambda_{exc.}$= 266, 313, and 334 nm respectively).[21] The quantum yield measurements were made in cyclohexane solution rather than *n*-heptane to allow comparisons with other quantum yield data obtained in our laboratories. It is unlikely that there will be any significant difference between quantum yield measurements in these two solvents. This confirms the presence of at least two, energetically close, excited states, the higher energy state being responsible for CO-loss. The TRIR measurements using $\lambda_{exc.}$ = 266 nm on (η^6-C$_6$H$_6$)Mo(CO)$_3$ showed a recovery of some 75% in the parent bleach over 800 ps. This would indicate an approximate quantum yield of 0.25 for the CO-loss process. Similar measurements using $\lambda_{exc.}$ = 400 nm yielded a value of 0.07. The behavior of the Mo system contrasts with that of the Cr, where the quantum yield of the CO-loss process decreases with reducing excitation wavelength.

The TRIR results obtained for (η^6-C$_6$H$_6$)Mo(CO)$_3$ should also be contrasted with those of the chromium system. Slow CO-loss is observed following both 266 and 400 nm excitation of (η^6-C$_6$H$_6$)Cr(CO)$_3$, whereas slow CO-loss is only observed following 266 nm irradiation of the (η^6-C$_6$H$_6$)Mo(CO)$_3$. Irradiation of (η^6-C$_6$H$_6$)Mo(CO)$_3$ at 400 nm produced excited-state bands that are different from those obtained for (η^6-C$_6$H$_6$)Cr(CO)$_3$, indicating a different excited-state structure. This is particularly noticeable for the high-frequency excited-state band that occurs to lower wavenumber relative to the parent in (η^6-C$_6$H$_6$)Cr(CO)$_3$ but to higher energy for (η^6-C$_6$H$_6$)Mo(CO)$_3$. These different excited states have a profound effect on the subsequent photoreactivity. The (η^6-C$_6$H$_6$)Mo(CO)$_3$ excited state (MACT$_2$) is nonreactive and relaxes to re-form the parent. In the 400 nm experiment there is some evidence for a weak band at 1966 cm^{-1}, and this could be because of the additional formation of a MACT$_1$ excited state similar to that observed in the chromium system. The second band of the MACT$_1$ state would be masked by the broad feature at 1894 cm^{-1}. The signal-to-noise ratio in these experiments does not permit further kinetic evaluation of the fate of these bands. These results indicate that the photochemistry of (η^6-C$_6$H$_6$)M(CO)$_3$ is complex and three different excited states may be involved.

The main difference in the TRIR results at 266 nm for (η^6-C$_6$H$_6$)Mo(CO)$_3$ are the production of two broad features at lower wavenumber than the parent bands. These bands decay to form (η^6-C$_6$H$_6$)Mo(CO)$_2$, and at later times there is evidence for bands at 1966 and ca. 1910 cm^{-1}, the latter band being obscured by the parent. These results are interpreted in terms of changes in the relative energies of excited states in the MACT$_1$ and MCCT/LF manifolds and a larger thermal barrier at the avoided crossing for the molybdenum complex compared to the chromium. More efficient CO-loss following 266 nm excitation can occur either by direct population of the MCCT/LF state (reaction (iii) in Scheme 1) or by a higher proportion of the reactive MACT$_1$ state possessing sufficient thermal energy to surmount the barrier at the avoided crossing; that is, 266 nm irradiation produces the MACT$_1$ state in a vibrationally excited state, resulting in CO-loss (reaction (ii) in Scheme 1).

Concluding Comments

These experiments demonstrate that a variety of competing photophysical processes must be considered to explain the photochemistry of these simple "half-sandwich" complexes. Nonradiative relaxation processes, vibrational cooling, and avoided crossing to unbound potential energy surfaces are all involved in explaining the remarkable diversity of the photochemical behavior for these systems. In Figure 7 a schematic representation of the ground- and excited-state potential energy surfaces are presented. For the chromium system CO-loss can occur following excitation at both 400 and 266 nm via an avoided crossing of MACT and MCCT/LF states. This leads to an unusually slow CO-loss. Rapid CO-loss is observed following 266 nm excitation because of direct population of the MCCT/LF state. The quantum yield for CO-loss in the chromium system decreases with increasing excitation energy because of the competing population of a high-energy unreactive

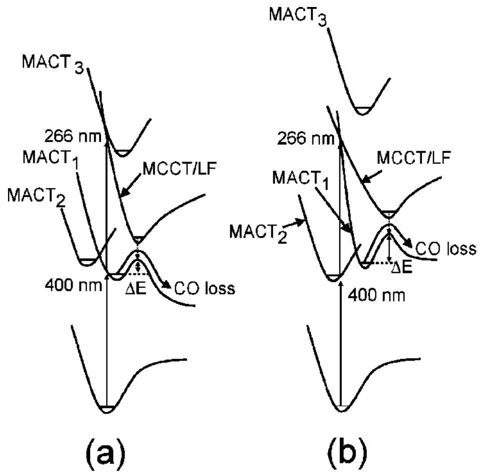

Figure 7. Potential energy cross sections for the ground and optically accessible excited states of $(\eta^6\text{-}C_6H_6)M(CO)_3$ ((a) M = Cr; (b) M = Mo). The vertical solid arrows indicate the excitation processes. The energy barrier at the avoided crossing of $MACT_1$ and MCCT/LF states results in a thermal barrier (ΔE), which is small for M = Cr but larger for M = Mo.

MACT state. For the molydenum system CO-loss is a minor process for 400 nm excitation, and an unreactive MACT state is evident from the TRIR spectra. A higher quantum yield for CO-loss is observed following 266 nm excitation through both direct population of the MCCT/LF state and production of a vibrationally excited reactive MACT state. This results in the quantum yield for CO-loss increasing with increasing excitation energy. No information on the spin multiplicity of the excited states was obtained during the course of this work however. It should be noted that it has been proposed that the photoinduced CO-loss from $Cr(CO)_6$ occurs via a singlet excited state.[34] There is clearly more to learn regarding the photophysics and photochemistry of these systems including the multiplicity of the excited state. The combination of DFT and time-resolved spectroscopy is likely to be useful in this regard.

Experimental Section

The matrix isolation apparatus has been described in detail elsewhere.[35] It consists of a HC2 closed helium displex refrigerator supplied by APD Cryogenics in thermal contact with a CaF_2 optical flat, contained within a stainless steel shroud equipped with CaF_2 windows. The temperature of the matrix was maintained by a heating current controlled by a Lakeshore 330 analog temperature control unit The optical flat was capable of rotation through 90°, allowing it to alternatively face the sample vapor/isolating gas streams and the monitoring spectrophotometers. The shroud vacuum was achieved by a combination of dual-stage rotary pumps backing an oil diffusion pump fitted with a liquid N_2 coldfinger trap. Typically a shroud vacuum of 2×10^{-6} Torr was achieved at a sample-plate temperature of 20 K. Perkin-Elmer Spectrum One FTIR (typically 16 scans at 4 cm^{-1} resolution) and Lambda EZ201 UV/visible spectrometers were used to monitor the spectral changes during the experiments. The isolating gas was admitted to the cold sample-plate via a needle value system connected to a stainless-steel gas-mixing line. The isolating gases were obtained from Cryogenics. Oriel Instruments supplied the light sources, which were either a 200 W Xe or Xe−Hg lamp, the former for broadband and the latter for monochromatic irradiations. Suitable interference filters were used to select the required Hg spectral line for monochromatic irradiations.

The initial experiments were performed on the TRIR apparatus based at the Rutherford Appleton Laboratory (RAL), which has been described in detail elsewhere.[36,37] The later experiments and the ones reported here were performed using TRIR apparatus located at Nottingham University, which is based on the PIRATE apparatus. A commercial Ti:sapphire oscillator (MaiTai)/regenerative amplifier system (Spitfire Pro) (Spectra Physics) is used to generate 800 nm laser pulses with an energy of 2.3 mJ at a repetition rate of 1 kHz. This output is divided into two parts with approximately the same energy pumping either a TP-1 harmonic generator (TimePlate Tripler, Minioptic Technology, Inc.) to generate UV pulses (400 or 267 nm) or a TOPAS-C OPA (light conversion) with a DFG (difference frequency generator) unit to produce a tunable mid-IR pulse with a spectral bandwidth of 180 cm^{-1} and the pulse energy of ca. 2 μJ at 2000 cm^{-1}. The IR pulse passes through a Ge beam splitter, and half of the IR pulse is reflected onto a single-element MCT detector (Kolmar Technology) to serve as a reference; the other half serves as the probe beam, which is focused and overlaps with the pump beam at the sample position. The UV−vis pump pulse is optically delayed (up to 3 ns) by a translation stage (LMA Actuator, Aerotech) and focused onto the sample with a quartz lens. The polarization of the pump pulse is set at the magic angle (54.7°) relative to the probe pulse to recover the isotropic absorption spectrum. For a measurement with a longer time delay, a Q-switched Nd:YVO laser (ACE-25QSPXHP/MOPA, Advanced Optical Technology, UK) is employed as a pump source, which is synchronized to the Spitfire Pro amplifier. The delay between pump and probe pulses can be controlled with a pulse generator (DG535, Stanford Research System) from 0.5 ns to 100 μs. The broadband transmitted probe pulse is detected with a HgCdTe array detector (Infrared Associates), which consists of 128 elements (1 mm high, 0.25 mm wide). The array detector is mounted in the focal plane of a 250 mm IR monochromator (DK240, Spectra Product) with 150 and 300 L/mm gratings, resulting in spectral resolutions of ca. 4 and ca. 2 cm^{-1}, respectively, at 2000 cm^{-1}. The signals from the array detector elements and the single-element detector were amplified with a 144-channel amplifier and digitized by a 16-bit analog-to-digital converter (IR-0144, Infrared Systems Development Corporation). The pump-induced change in the absorbance (ΔA) is determined by chopping the pump pulse at half the repetition frequency of the laser and calculating the ratio between the pump-on and pump-off transmittance. Chopping the excitation light pulse greatly reduces long-term instrumental drift. The signal from the single-element detector serves as reference to normalize the shot to shot fluctuation. The pump beam size (~500

---

(34) Trushin, S. A.; Kosma, K.; Fuss, W.; Schmid, W. E. *Chem. Phys.* **2008**, *347*, 309–323.

(35) Long, C.; Maher, K.; Pryce, M. T. *J. Organomet. Chem.* **2006**, *691*, 3298–3304.

(36) Towrie, M.; Parker, A. W.; Shaikh, W.; Matousek, P. *Meas. Sci. Technol.* **1998**, *9*, 816–823.

(37) Towrie, M.; Grills, D. C.; Dyer, J.; Weinstein, J. A.; Matousek, P.; Barton, R.; Bailey, P. D.; Subramaniam, N.; Kwok, W. M.; Ma, C. S.; Phillips, D.; Parker, A. W.; George, M. W. *Appl. Spectrosc.* **2003**, *57*, 367–380.

(38) Frisch, M. J.; Trucks, G. W.; Schlegel, H. B.; Scuseria, G. E.; Robb, M. A.; Cheeseman, J. R.; Montgomery, J. J. A.; Vreven, T.; Kudin, K. N.; Burant, J. C.; Millam, J. M.; Iyengar, S. S.; Tomasi, J.; Barone, V.; Mennucci, B.; Cossi, M.; Scalmani, G.; Rega, N.; Petersson, G. A.; Nakatsuji, H.; Hada, M.; Ehara, M.; Toyota, K.; Fukuda, R.; Hasegawa, J.; Ishida, M.; Nakajima, T.; Honda, Y.; Kitao, O.; Nakai, H.; Klene, M.; Li, X.; Knox, J. E.; Hratchian, H. P.; Cross, J. B.; Adamo, C.; Jaramillo, J.; Gomperts, R.; Stratmann, R. E.; Yazyev, O.; Austin, A. J.; Cammi, R.; Pomelli, C. J.; Ochterski, W.; Ayala, P. Y.; Morokuma, K.; Voth, G. A.; Salvador, P.; Dannenberg, J. J.; Zakrzewski, V. G.; Dapprich, S.; Daniels, A. D.; Strain, M. C.; Farkas, O.; Malick, D. K.; Rabuck, A. D.; Raghavachari, K.; Foresman, J. B.; Ortiz, J. V.; Cui, Q.; Baboul, A. G.; Clifford, S.; Cioslowski, J.; Stefanov, B. B.; Liu, G.; Liashenko, A.; Piskorz, P.; Komaromi, I.; Martin, R. L.; Fox, D. J.; Keith, T.; Al-Laham, M. A.; Peng, C. Y.; Nanayakkara, A.; Challacombe, M.; Gill, P. M. W.; Johnson, B.; Chen, W.; Wong, M. W.; Gonzalez, C.; Pople, J. A. *Gaussian 03, Revision C.02*; Gaussian, Inc.: Wallingford, CT, 2004.

μm diameter) is larger than the probe spot (~200 μm diameter) to ensure spatially uniform photoexcitation over the area of the probe pulse. A Harrick flowing solution cell with 2-mm-thick CaF_2 windows (path length 0.5 mm) is mounted on a motorized cell mount, which moves the cell rapidly in x and y dimensions throughout the experiment. Consequently each laser pulse illuminates a different volume of the sample, reducing overheating and degradation of the sample solution and cell windows.

All calculations were carried out using the Gaussian 03 program revision C.02[38] running on a dual Xeon processor workstation (3.6 GHz) under Windows XP. All calculations used the Becke three-parameter hybrid functionals,[39] using the correlation function of Lee, Yang, and Parr, which includes both local and nonlocal terms.[40] The LANL2DZ and LANL2DZ+P basis set was used for all calculations, which employs the Dunning/Huzinaga valence double-ζ functions for the first-row elements,[41] and the Los Alamos effective core potentials plus double-ζ functions on elements from Na to Bi.[42−44] An additional polarization function (+P) was added to the chromium atom for calculations on the reduced hapticity species to ensure compatibility with the published data.[45,46] Time-dependent DFT calculations used the structure obtained from an optimization at the B3LYP/LANL2DZ model chemistry. The TDDFT calculations examined only the 20 lowest energy singlet states. The GaussSum package[47] was used to obtain the contribution to specific Kohn−Sham orbitals made by specific molecule fragments, namely, the three CO ligands, the metal atom, and the benzene ligand (see Supporting Information for details).

Acknowledgment. We thank the EPSRC for funding. The authors acknowledge the many helpful discussions with Dr. D. Brougham (DCU) on theoretical aspects of this work. The authors thank the EU Framework 6 Programme for support in accessing the PIRATE system at RAL. Louth County Council is thanked for support for N.M.B. M.W.G. gratefully acknowledges receipt of a Royal Society Wolfson Merit Award.

Supporting Information Available: This material is available free of charge via the Internet at http://pubs.acs.org.

OM800925S

---

(39) Becke, A. D. *J. Chem. Phys.* **1993**, *98*, 5648–5652.

(40) Lee, C. T.; Yang, W. T.; Parr, R. G. *Phys. Rev. B* **1988**, *37*, 785–789.

(41) Dunning Jr, T. H.; Hay, P. J. In *Modern Theoretical Chemistry*, Schaefer, H. F., III, Ed.; Plenum Press: New York, 1977; Vol. 3.

(42) Hay, P. J.; Wadt, W. R. *J. Chem. Phys.* **1985**, *82*, 270–283.

(43) Wadt, W. R.; Hay, P. J. *J. Chem. Phys.* **1985**, *82*, 284–298.

(44) Hay, P. J.; Wadt, W. R. *J. Chem. Phys.* **1985**, *82*, 299–310.

(45) Hoellwarth, A.; Boehme, M.; Dapprich, S.; Ehlers, A. W.; Gobbi, A.; Jonas, V.; Koehler, K. F.; Stegmann, R.; Veldkamp, A.; Frenking, G. *Chem. Phys. Lett.* **1993**, *208*, 237–240.

(46) Ehlers, A. W.; Boehme, M.; Dapprich, S.; Gobbi, A.; Hoellwarth, A.; Jonas, V.; Koehler, K. F.; Stegmann, R.; Veldkamp, A.; Frenking, G. *Chem. Phys. Lett.* **1993**, *208*, 111–114.

(47) O'Boyle, N. M. *GaussSum 2.0*; 2006.